SUPPORTING INFORMATION

Spin Multiplicity and Solid State Electrochemical Behaviour in Charge Transfer Co-crystals of DBTTF:F4TCNQ

Federica Solano[1], Paolo Inaudi[2], Mario Chiesa[1], Gabriele Kociok-Kohn[3], Enrico Salvadori[1], Enrico Da Como[4*], Davide Vanossi[5], Mery Malandrino[1], Raanan Carmieli[6], Agnese Giacomino*[2], Claudio Fontanesi[7]

[1] Department of Chemistry, University of Torino, Via Giuria 5, Torino, Italy

[2] Department of Drug Science and Technology, University of Torino, Via Giuria 9, Torino, Italy

[3] Material and Chemical Characterization Facility (MC^2), University of Bath, Claverton Down, Bath BA2 7AY, United Kingdom

[4] Centre for Photonics and Photonic Materials (CPPM) and Department of Physics, University of Bath, BA2 7AY, United Kingdom

[5] DSCG, University of Modena and Reggio Emilia, via Campi 183, 41125, Modena, Italy

[6] Department of Chemical and Biological Physics, Weizmann Institute of Science, Rehovot 76100 Israel

[7] DIEF, University of Modena and Reggio Emilia, via Vivarelli 10, 41125 Modena, Italy

* Corresponding author (e-mail: agnese.giacomino@unito.it; edc25@bath.ac.uk)

Contents

1. Estimation of HOMO and LUMO from E_{ONSET}

Energy of HOMO and LUMO were calculated from E_{ONSET} [1] as

HOMO=- *Eonset,ox* (4,8 – *Eonset,ox fc*) [eV]

LUMO= - *E onset,red* (4,8 – *Eonset,ox fc*) [eV]

2. Q-band EPR spectrum

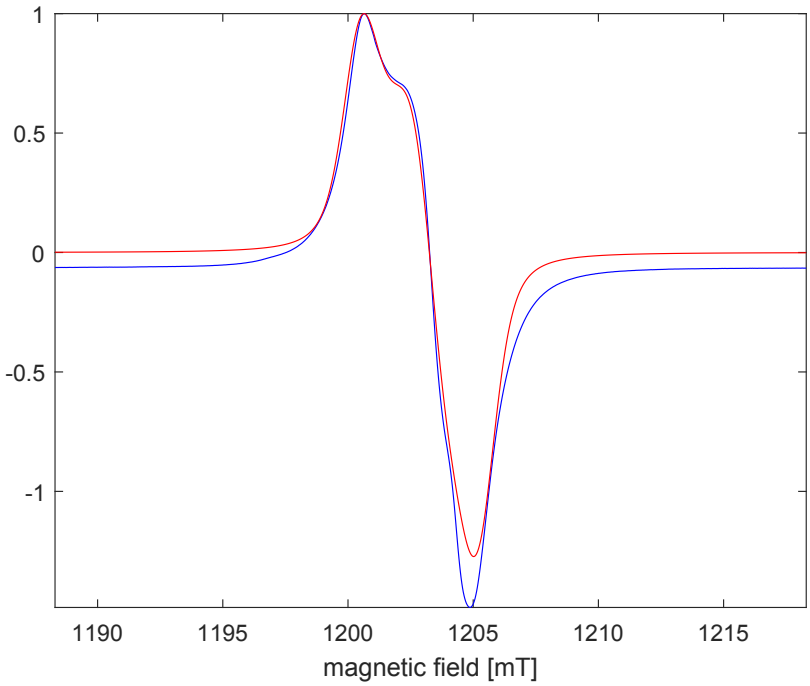

Figure S1. Experimental (blue) and simulated (red) Q-band CW EPR spectrum of DBTTF:F4TCNQ co-crystals recorded at 50 K. The spectrum was recorded at 25 dB attenuation and a modulation amplitude of 0.1 mT. The simulation of the spectrum was obtained using the following spin-Hamiltonian $\hat{\mathcal{H}} = \mu_B \mathbf{S}\mathbf{g}B$ for a S=1/2 species with **g** tensor **g**= [2.0027 2.0059 2.0105]. DFT calculated value **g** tensor (DBTTF)= [2.0021370 2.0064689 2.0106794]

Table S1. Calculated g-tensor values, CAMB3LYP/6-31(d,p) level of theory. DBTTF radical cation, F4TCNQ radical anion species.

	g1	*g2*	*g3*
DBTTF	2.0021370	2.0064689	2.0106794
F4TCNQ	2.0030361	2.0028716	2.0023441

3. Electrochemical behaviour of pristine F4TCNQ, DBTTF in solutions

This analysis was performed using PalmSens3 portable potentiostat (PalmSens, Houten, Netherlands) interfaced with the software PSTrace 4.6. Figure S2 and S3 show CV curves recorded for the pristine F4TCNQ and DBTTF organic compounds in 0.1 TBAPF6 AN solution, using a GCE as WE, with a diameter of 3 mm, a Pt electrode as CE and Ag/AgCl/KClsat as RE. CVs were recorded for three different scan rate, 20, 50 and 100 mV s^{-1}, respectively. This set up has been used for all anlysis in solution.

F4TCNQ. Figure S2 shows the CVs obtained for F4TCNQ. The profile is in good agreement with data already reported in the literature[2-4]. Two reduction/oxidation peaks are present in the forward-negative/backward-positive potential scan direction, they are of reversible nature with a peak-to-peak separation of about 60 mV, which remains almost constant at different scan rate values. All in all, the first two reduction processes appear fast and reversible. Table S1 describes oxidation-reductive processes of F4TCNQ solution and Table S2 summarizes the F4TCNQ peaks and standard potential values. Table S3 reports LUMO values comparable to those in literature[2-4].

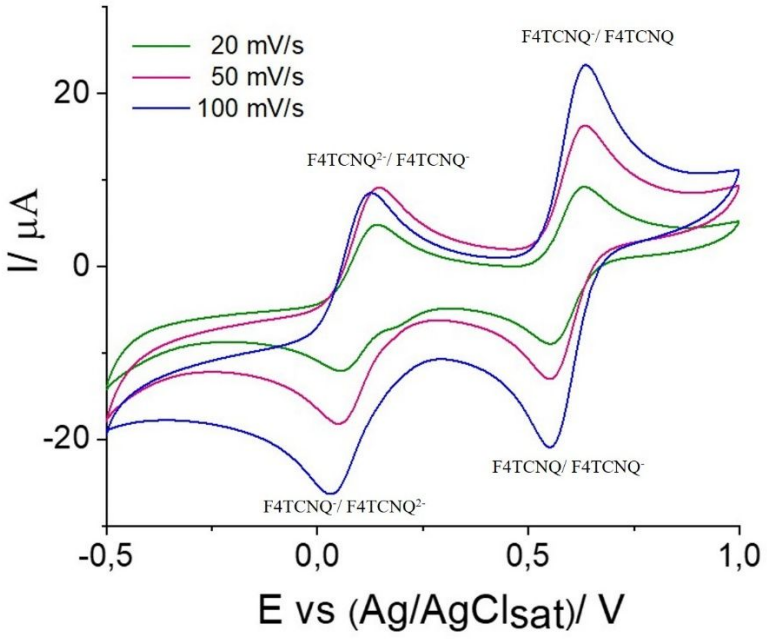

Figure S2. CV voltammogram of 1 mM F4TCNQ in 0.1 M TBAPF6 ACN solution, CE: Pt wire. Green, red and blue CV profiles were obtained at 20, 50, 100 mV s^{-1} scan rate, respectively.

Table S2. Oxidation-reductive processes of F4TCNQ

$F4TCNQ_{sol} + e^-$	⇄	$F4TCNQ^{1-}_{sol}$	Ep^2
$F4TCNQ^{1-}_{sol} + e^-$	⇄	$F4TCNQ^{2-}_{sol}$	Ep^1

Table S3. E, ΔE and$E_{1/2}$ measured for F4TCNQ at 20, 50, 100 mV s^{-1}

Scan rate	*E (V)*	*ΔE (V)*	*E1/2 (V)*
20 mV s^{-1}			
$E_{pa}{}^1$	0.153	0.091	0.108
$E_{pc}{}^1$	0.062		
$E_{pa}{}^2$	0.640	0.097	0.597
$E_{pc}{}^2$	0.543		
50 mV s^{-1}			
$E_{pa}{}^1$	0.148	0.091	0.105
$E_{pc}{}^1$	0.057		
$E_{pa}{}^2$	0.640	0.086	0.600
$E_{pc}{}^2$	0.554		
100 mV s^{-1}			
$E_{pa}{}^1$	0.118	0.086	0.088
$E_{pc}{}^1$	0.032		
$E_{pa}{}^2$	0.645	0.091	0.600
$E_{pc}{}^2$	0.554		

Table S4. $E_{onset,rid}$ and LUMO energy measured for of F4TCNQ at 20, 50, 100 mV s^{-1}

Scan rate	$E_{onset, rid}$ F4TCNQ /F4TCNQ$^-$ (V)	LUMO (eV)
20 mV/s	0.667	-5.167
50 mV/s	0.656	-5.147
100 mV/s	0.664	-5.154

DBTTF. Figure S3 sets out DBTTF CV profiles. Two oxidation peaks are present in the forward oxidation scan: these redox processes appear fast and reversible, with a peak-to-peak separation of about 60 mV. Table S5 shows the relevant current peak and standard potentials. A third broad current peak is present at a potential around +1.4 V, that shows an irreversible nature (possibly due to the initial stage of a polymerization reaction, which is typical of thiophene derivatives[5,6]. Few electrochemical studies about DBTTF are present in the literature; in any case the obtained results are in quantitative agreement with the data reported[7]. To the best of our knowledge, this paper reports for the first time CV voltammograms of DBTTF. The values of HOMO present in the Table S6 are in excellent agreement with those reported by Li et al., 2012 [8].

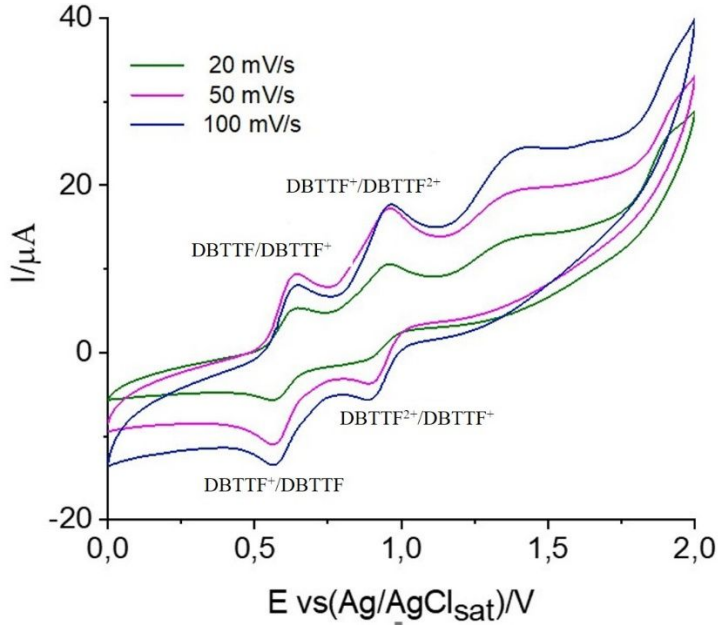

Figure S3. CV voltammograms of 1 mM DBTTF in 0.1 M TBAPF6 ACN solution, CE: Pt wire. Green, red and blue CV profiles were obtained at 20, 50, 100 mV s^{-1} scan rate, respectively.

Table S5. Oxidation-reductive processes of DBTTF

$DBTTF_{sol}$	$\rightleftarrows$	$DBTTF^{1+}_{sol} + e^-$	$E_p{}^1$
$DBTTF^{1+}_{sol}$	$\rightleftarrows$	$DBTTF^{2+}_{sol} + e^-$	$E_p{}^2$

Table S6. E, ΔE, $E_{1/2}$ to 20, 50, 100 mV s^{-1} DBTTF

	E (V)	*ΔE (V)*	*$E_{1/2}$ (V)*
20 mV s^{-1}			
E_{pa}^{1}	0.639	0.074	0.602
E_{pc}^{1}	*0.565*		
E_{pa}^{2}	0.957	0.070	0.922
E_{pc}^{2}	*0.887*		
E_{pa}^{3} *polymerization*	*1.398*		
50 mV s^{-1}			
E_{pa}^{1}	0.648	0.076	0.610
E_{pc}^{1}	0.572		
E_{pa}^{2}	0.967	0.060	0.937
E_{pc}^{2}	0.907		
E_{pa}^{3} *polymerization*	1.400		
100 mV s^{-1}			
E_{pa}^{1}	0,653	0.091	0.607
E_{pc}^{1}	0.562		
E_{pa}^{2}	0.973	0.076	0.935
E_{pc}^{2}	0.897		
E_{pa}^{3} *polymerization*	1.403		

Table S7. $E_{onset,rid}$ and HOMO of DBTTF to 20, 50, 100 mV s^{-1}

Scan rate	*$E_{onset, ox}$ DBTTF/DBTTF^{+} (V)*	*HOMO (eV)*
20 mV s^{-1}	0.568	-5.068
50 mV s^{-1}	0.553	-5.044
100 mV s^{-1}	0.561	-5.051

Table S8. Summarizes the electrochemical results of the pristine F4TCNQ and DBTTF at 20 mV s^{-1} potential scan rate.

20 (mV s^{-1}) *scan rate*	*E_{pa} (V)*	*E_{pc} (V)*	*ΔE (V)*	*HOMO (eV)*	*LUMO (eV)*
$F4TCNQ_{(sol)} + e^- \rightleftharpoons F4TCNQ^-_{(sol)}$	0.640	0,543	0.097		-5.167
$F4TCNQ^-_{(sol)} + e^- \rightleftharpoons F4TCNQ^{2-}_{(sol)}$	0.153	0.062	0.091		
$DBTTF_{(sol)} \rightleftharpoons DBTTF^+_{(sol)} + e^-$	0.639	0.565	0.074	-5.068	
$DBTTF^+_{(sol)} \rightleftharpoons DBTTF^{2+}_{(sol)} + e^-$	0.957	0.887	0.070		

4. Electrochemical behaviour of solid pristine F4TCNQ, DBTTF

This analysis was performed using PalmSens3 portable potentiostat (PalmSens, Houten, Netherlands) interfaced with the software PSTrace 4.6. Figure S4 shows CV curves recorded for the solid pristine DBTTF using a cylindrical teflon cell featuring a hole (0.8 cm diameter), the glassy carbon flat as WE, AN solution using TBAPF6 as supporting electrolyte and nafion membrane to prevent direct contact between the solid pristine and the electrolytic solution. CVs were recorded for three different scan rate, 20, 50 and 100 mV s^{-1}, respectively. The voltammogram in solution and solid state are comparable despite different working conditions: two pairs of peaks are always observed indicative of the two reversible reactions to an electron, this time shifted to more positive potentials. This highlights the reliability of solid state electrochemistry on flat cell. the DBTTF polymerisation peak observed in the 1.3 V solution voltammogram has disappeared. From this it is clear the advantage of an analysis in solid state that is the reduction of the phenomena of interference involved to solution.

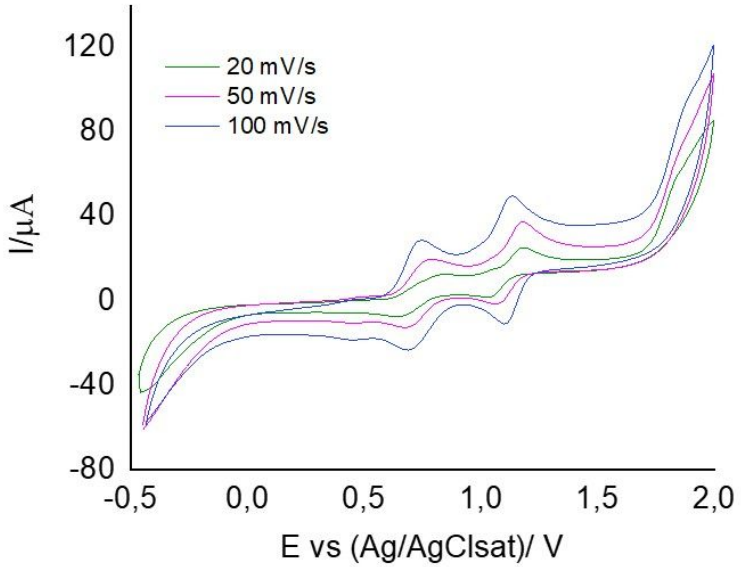

Figure S4. CV of 1 mg DBTTF powder covered with a nafion membrane, 0.1 M TBAPF6 AN solution, glassy carbon plate WE, Pt wire the CE, Ag/AgCl/KCl RE. 20 50 100 mV s^{-1} scan rate.

Table S9. E, ΔE, $E_{1/2}$ to 20, 50, 100 mV s^{-1} DBTTF powder

	E (V)	*ΔE (V)*	*$E_{1/2}$ (V)*

20 mV s^{-1}			
E_{pa}	0.821	0.152	0.745
E_{pc}	*0.669*		
E_{pa}	1.186	0.126	1.123
E_{pc}	*1.060*		
50 mV s^{-1}			
E_{pa}	0.792	0.102	0.741
E_{pc}	0.690		
E_{pa}	1.197	0.121	1.137
E_{pc}	1.076		
100 mV s^{-1}			
E_{pa}	0.740	0.046	0.717
E_{pc}	0.694		
E_{pa}	1.135	0.025	1.122
E_{pc}	1.110		

In the case of F4TCNQ, registration of the CV in solid state was not possible. This was due to the p-type dopant effect of F4TCNQ against the nafion layer. This reaction is clearly visible by the sudden bright green colouring of the solution inside the cell. What happens is a doping of the F4TCNQ caused by the strong interaction with the side chains of the nafion.

Ion pairs are formed between the electron of F4TCNQ and the hole in the polymer which increases its conductivity.

5. Stability of pristine F4TCNQ, DBTTF through CVs and UV-Vis techniques

A systematic study on F4TCNQ, DBTTF time dependent stability in the adopted experimental conditions was carried out by recording both CVs and UV-Vis spectra as a function of time.

This analysis was performed using PalmSens3 portable potentiostat (PalmSens, Houten, Netherlands) interfaced with the software PSTrace 4.6, using a GCE as WE, with a diameter of 3 mm, a Pt electrode as CE and Ag/AgCl/KClsat as RE. CVs of F4TCNQ 1 mM in AN solution, 0.1 M TBAPF6 was monitored for 68 h.

The UV-Vis spectrum were obtained using a Jasco V-550 UV-Vis (JASCO Corporation, Tokyo, Japan) interfaced with a computer. UV-Vis spectrum of F4TCNQ $4x10^{-3}$ mM in AN solution, 0.4 mM TBAPF6 was monitored from 0 to 68 h.

The stability study allowed to ensure a total reliability of our electrochemical measurements, which were run on a much shorter time scale with respect to the start of any degradation reaction.

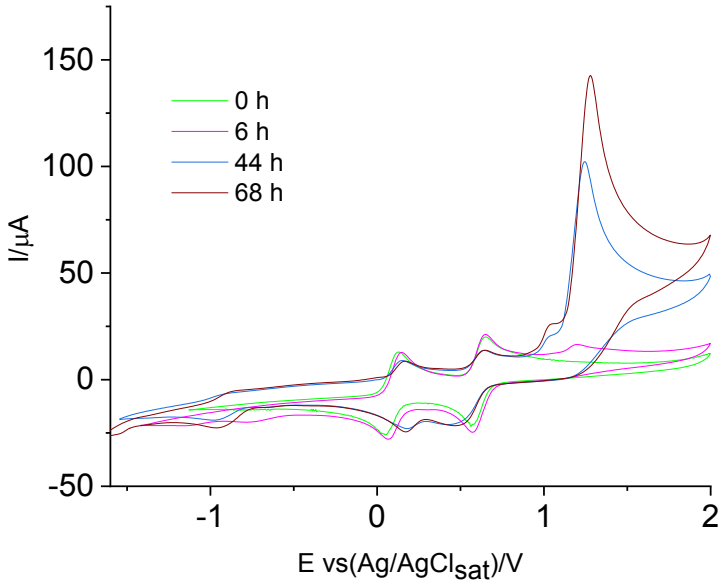

Figure S5. CVs of F4TCNQ 1 mM in AN solution, 0.1 M TBAPF6 monitored from 0 to 68 h

F4TCNQ is characterized by some chemical stability issue, likely related to the reactivity of the cyano groups with water. The Figure S5 sets out CVs of the monitored F4TCNQ solution in a time from 0 to 68 h. This analysis shows the degradation of F4TCNQ over time. This is observable with the formation of a third irreversible peak of oxidation at 1.4 V which corresponds to the rupture of the cyan group resulting in the formation of $CN^{\bullet}$ radicals. The reduction peak moves to lower potentials sign of loss of cyan groups, strong electron-attractors[5].

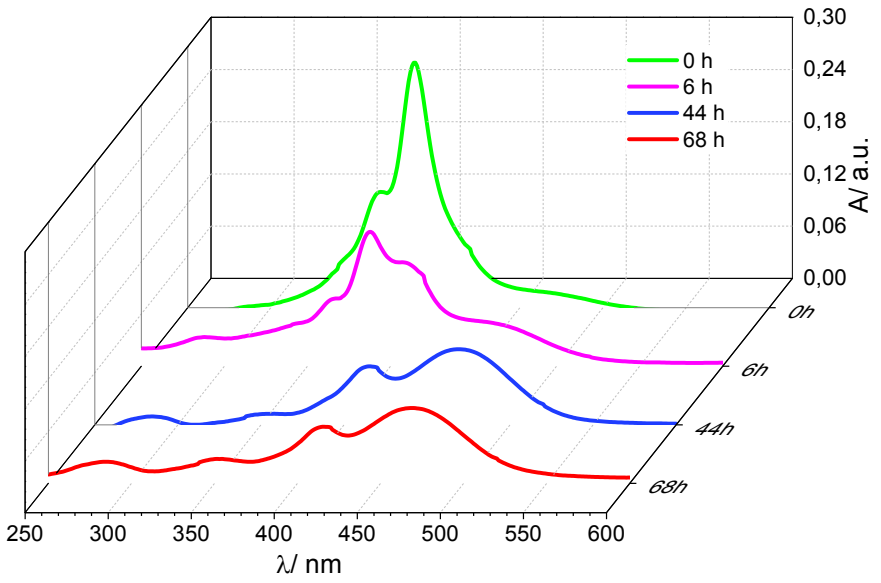

Figure S6. UV-Vis spectrum of F4TCNQ $4x10^{-3}$ mM in AN solution, 0.4 mM TBAPF6 monitored from 0 to 68 h

The Figure S6 shows the UV-Vis spectrum of the monitored F4TCNQ solution in a time from 0 to 48 h. The data in Figure S7 at 0 time are in good agreement with data already reported in the literature[9]. F4TCNQ degradation is confirmed by UV-Vis analysis where a substantial change to the characteristic absorption band can be detected.

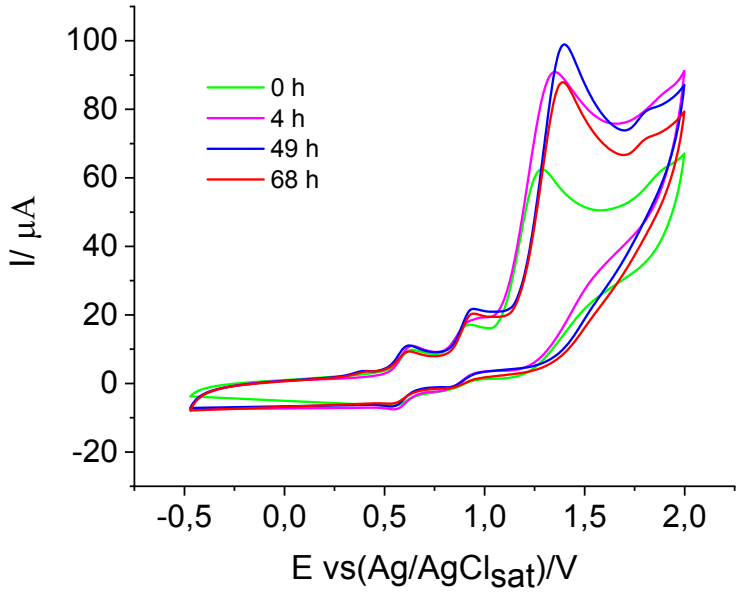

Figure S7. CVs of DBTTF 1 mM in AN solution, 0.1 M TBAPF6 monitored from 0 to 68 h

The Figure S7 shows CVs of DBTTF solution monitored for 68 h. The CVs indicate a considerable increase in the phenomenon of polymerization. This is observable from increase in peak current at a potential around +1.4 V, which basically of irreversible nature[10].

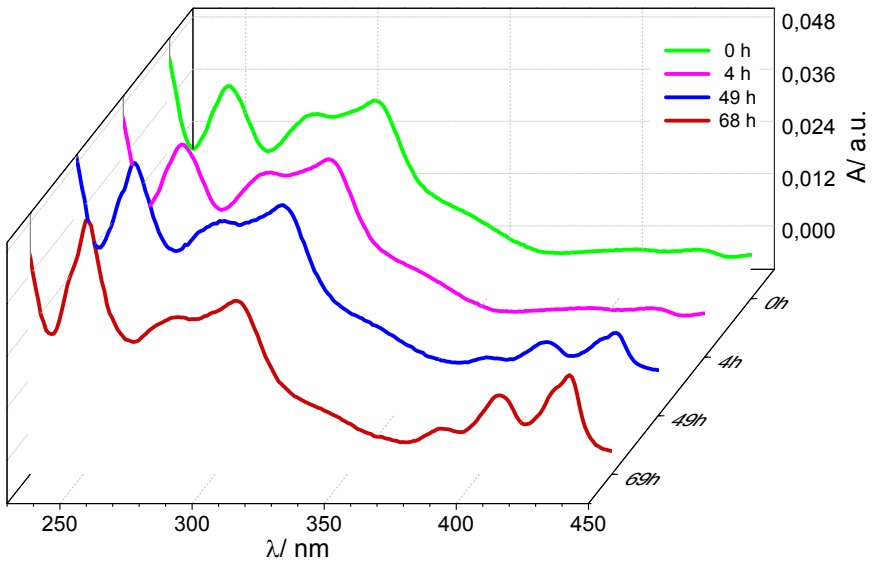

Figure S8. UV-Vis spectrum of DBTTF 4x10^{-3} mM in ACN solution, 0.4 mM TBAPF6 monitored from 0 to 68 h

In Figure S8 we show the UV-Vis spectrum of the DBTTF solution in a time interval from 0 to 48 h. The formation of two bands at 410 and 440 nm is probably linked to the polymerization phenomenon.

6. Affinity between donor and acceptor

Donor and acceptor were added simultaneously in the same AN solution, 0.1 M TBAPF6 to demonstrate their strong affinity. The solution was analyzed through a conventional three electrode cell using a GCE as WE, with a diameter of 3 mm, a Pt electrode as CE and Ag/AgCl/KClsat as RE.We observed, the instantaneous formation of a precipitate. This indicates the strong polarity of formed complex. The electrochemical (Fig. S9) and UV-Vis (Fig. S10) response of the materials left in solution seem to be the sum of the response from the two pristine compounds, indicating that some uncomplexed species remain in solution[3].

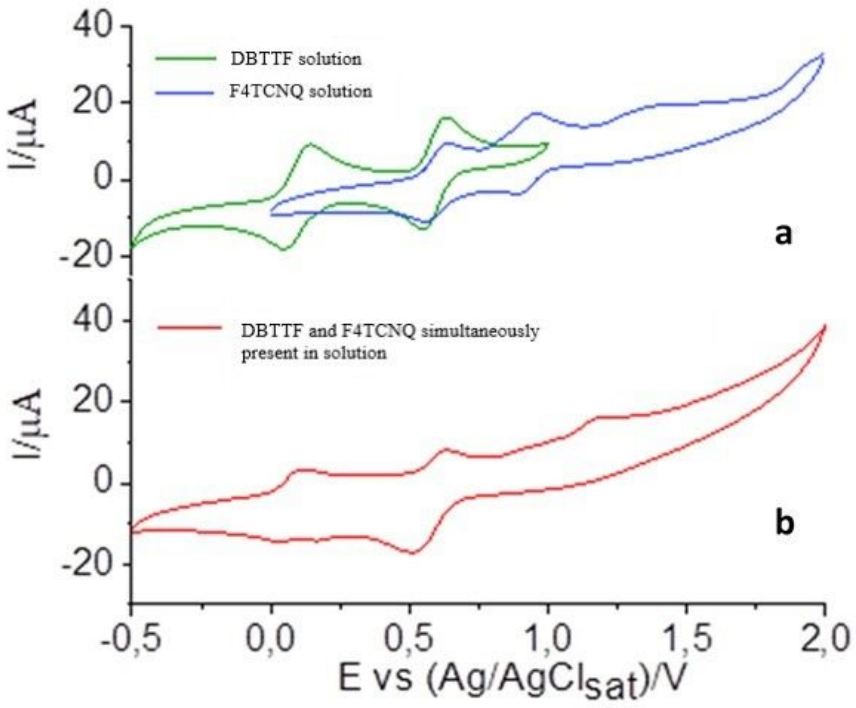

Figure S9. a) CVs of the 1mM F4TCNQ and 1mM DBTTF compounds in 0.1 M $TBAPF_6$ ACN solution. b) CV of the 0.1 mM DBTTF and 0.1mM F4TCNQ simultaneously in solution. WE: GCE, RE: $Ag/AgCl/KCl_{sat}$, CE: Pt wire. 50 mV s^{-1} is the potential scan rate.

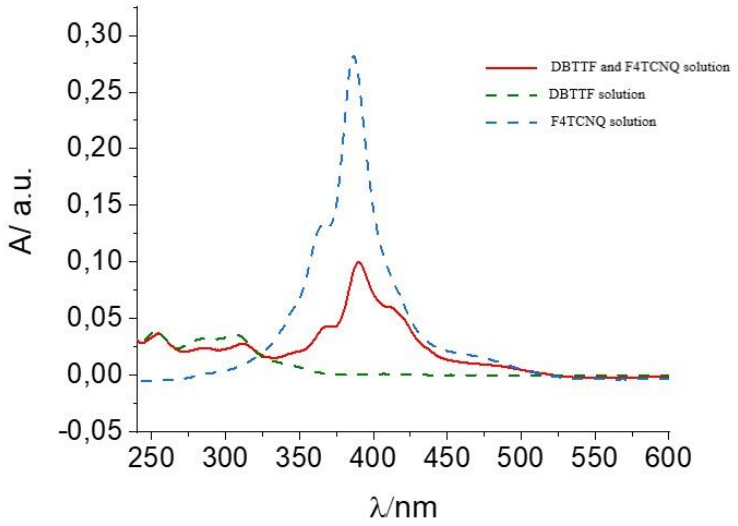

Figure S10. UV-Vis spectrum of green $4x10^{-3}$ mM F4TCNQ solution (green spectrum), $4x10^{-3}$ mM DBTTF solution (blue spectrum) and $2x10^{-3}$ mM DBTTF and F4TCNQ simultaneously in solution (red spectrum)

7. CVs of Co-crystals to 20 50 100 mV s^{-1} scan rate

The following are the CVs of DBTTF:F4TCNQ co-crystal in the 0.0 to 1.6 V potential range, Figure S11 a), and CVs of DBTTF:F4TCNQ co-crystal recorded starting from the OCP to anodic and cathodic scans, Figure S11 b). CV curves recorded using a cylindrical teflon cell featuring a hole (0.8 cm diameter), the glassy carbon flat as WE, AN solution using TBAPF6 as supporting electrolyte and nafion membrane. CVs were recorded for three different scan rate, 20, 50 and 100 mV s^{-1}, respectively.

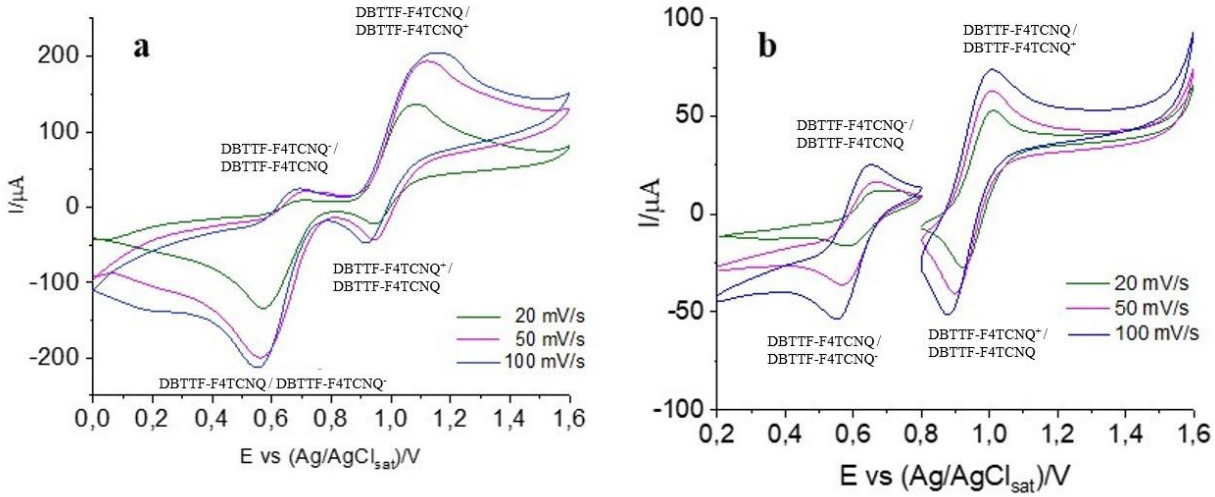

Figure S11. a) CVs of DBTTF:F4TCNQ co-crystal in the 0.0 to 1.6 V potential range ~~16~~b)CVs of DBTTF:F4TCNQ co-crystal recorded starting from the OCP to anodic and cathodic scans. 20 50 100 mV s^{-1} scan rate.

Table S10. Oxidation-reductive processes of DBTTF:F4TCNQ co-crystal

$DBTTF{:}F4TCNQ_{(solid)}$	⇄	$DBTTF{:}F4TCNQ^{+}_{(solid)} + e^{-}$	$E_p{}^2$
$DBTTF{:}F4TCNQ_{(solid)} +$	⇄	$DBTTF{:}F4TCNQ^{-}_{(solid)}$	$E_p{}^1$

TableS11. E, ΔE, $E_{1/2}$ to 20, 50, 100 mV s^{-1} of DBTTF:F4TCNQ co-crystal

Scan rate	*E (V)*	*ΔE (V)*	*$E_{1/2}$ (V)*
20 mV/s			
$E_{pa}{}^1$	*0.667*	*0.080*	*0.627*
$E_{pc}{}^1$	*0.587*		
$E_{pa}{}^2$	*1.017*	*0.100*	*0.971*
$E_{pc}{}^2$	*0.925*		
50 mV/s			
$E_{pa}{}^1$	*0.661*	*0.085*	*0.618*
$E_{pc}{}^1$	*0.576*		
$E_{pa}{}^2$	*1.005*	*0.108*	*0.948*
$E_{pc}{}^2$	*0.897*		
100 mV/s			
$E_{pa}{}^1$	*0.650*	*0.099*	*0.600*
$E_{pc}{}^1$	*0.551*		
$E_{pa}{}^2$	*1.011*	*0.134*	*0.944*
$E_{pc}{}^2$	*0.877*		

Table S11. Eonset, HOMO, LUMO and Band Gap of DBTTF:F4TCNQ co-crystal to 20, 50, 100 mV s-1

Scan rate	E_{onset} *(V)*	*HOMO (eV)*	*LUMO (eV)*	*Band gap (eV)*
20 mV s^{-1}				
$DBTTF{:}F4TCNQ_{(solid)} \rightleftharpoons DBTTF{:}F4TCNQ^{+}_{(solid)} +$	0.919	-5.249		0.249
$DBTTF{:}F4TCNQ_{(solid)} + e^{-} \rightleftharpoons DBTTF{:}F4TCNQ^{-}_{(sol}$	0.670		-5.000	
50 mV s^{-1}				
$DBTTF{:}F4TCNQ_{(solid)} \rightleftharpoons DBTTF{:}F4TCNQ^{+}_{(solid)} +$	0.900	-5.222		0.228
$DBTTF{:}F4_{(solid)} + e^{-} \rightleftharpoons DBTTF{:}F4^{-}_{(solid)}$	0.670		-4.994	
100 mV s^{-1}				
$DBTTF{:}F4TCNQ_{(solid)} \rightleftharpoons DBTTF{:}F4TCNQ^{+}_{(solid)} +$	0.899	-5.236		0.233
$DBTTF{:}F4TCNQ_{(solid)} + e^{-} \rightleftharpoons DBTTF{:}F4TCNQ^{-}_{(sol}$	0.670		-5.003	

References

(1) Sun, S.-S., Dalton, L.R., n.d. Introduction to Organic Electronic and Optoelectronic Materials and Device, 1st Edition 2008. ed, Optical science and engineering.

(2) Kataeva, O., Khrizanforov, M., Budnikova, Y., Islamov, D., Burganov, T., Vandyukov, A., Lyssenko, K., Mahns, B., Nohr, M., Hampel, S., et al. Crystal Growth, Dynamic and Charge Transfer Properties of New Coronene Charge Transfer Complexes. *Cryst. Growth Des.* **2016,** 16, 331–338. https://doi.org/10.1021/acs.cgd.5b01301

(3) Rainbolt, J.E., Koech, P.K., Polikarpov, E., Swensen, J.S., Cosimbescu, L., Von Ruden, A., Wang, L., Sapochak, L.S., Padmaperuma, A.B., Gaspar, D.J. Synthesis and characterization of p-type conductivity dopant 2-(3-(adamantan-1-yl)propyl)-3,5,6-trifluoro-7,7,8,8-tetracyanoquinodimethane. *J. Mater. Chem. C*, **2013,** 1, 1876. https://doi.org/10.1039/c3tc00068k

(4) Li, J., Zhang, G., Holm, D.M., Jacobs, I.E., Yin, B., Stroeve, P., Mascal, M., Moulé, A.J. Introducing Solubility Control for Improved Organic P-Type Dopants. *Chem. Mater.* **2015,** 27, 5765–5774. https://doi.org/10.1021/acs.chemmater.5b02340

(5) Fontanesi, C., Tassinari, F., Parenti, F., Cohen, H., Mondal, P.C., Kiran, V., Giglia, A., Pasquali, L., Naaman, R. New One-Step Thiol Functionalization Procedure for Ni by Self-Assembled Monolayers. *Langmuir*, **2015**, 31, 3546–3552. https://doi.org/10.1021/acs.langmuir.5b001776.

(6) Tassinari, F., Tancini, E., Innocenti, M., Schenetti, L., Fontanesi, C. On the Hybrid Glassy Carbon Electrode/OligoThiophene/Ag(NP) Interface. *Langmuir,* **2015**, 28, 15505–15512. https://doi.org/10.1021/la3025777

(7) Nagakubo, J., Ashizawa, M., Kawamoto, T., Tanioka, A., Mori, T. Stabilization of organic field-effect transistors by tert-butyl groups in dibenzotetrathiafulvalene derivatives. *Phys. Chem. Chem. Phys.* **2011**, 13, 14370. https://doi.org/10.1039/c1cp21507h

(8) Li, H., Wang, X., Li, Z. Theoretical study of the effects of different substituents of tetrathiafulvalene derivatives on charge transport. *Chin. Sci. Bull.* **2012**, 57, 4049–4056. https://doi.org/10.1007/s11434-012-5222-z

(9). Ma, L., Hu, P., Jiang, H., Kloc, C., Sun, H., Soci, C., Voityuk, A.A., Michel-Beyerle, M.E., Gurzadyan, G.G. Single photon triggered dianion formation in TCNQ and F4TCNQ crystals. *Sci. Rep.* **2016**, 6, 28510. https://doi.org/10.1038/srep28510

(10) Hu, P., Du, K., Wei, F., Jiang, H., Kloc, C. Crystal Growth, HOMO–LUMO Engineering, and Charge Transfer Degree in Perylene-F$_x$ TCNQ (x = 1, 2, 4) Organic Charge Transfer Binary Compounds. *Cryst. Growth Des.* **2016**, 16, 3019–3027. https://doi.org/10.1021/acs.cgd.5b01675